RSC Advances

PAPER

View Article Online
View Journal | View Issue

Cite this: RSC Adv., 2015, 5, 8669

Guided routing on spinning microfluidic platforms†

Amin Kazemzadeh,*[abc] P. Ganesan,[a] Fatimah Ibrahim,*[bc] Lawrence Kulinsky[d] and Marc J. Madou[de]

Flow directionality, valving and liquid routing in centrifugal microfluidics (Lab-on-CD) are typically controlled by applying centrifugal and Coriolis forces and have been the subject of active research interest in recent years. Determining and switching the flow direction at a T-junction is a common fluidic operation important for implementing several chemical and clinical assays for Lab-on-CDs. The present work describes a novel approach to route samples and control flow direction on a spinning disc that employs a guiding microstructure that relies on a two-stage valve comprised of an auxiliary inlet, which is a recess embedded at a T-junction, and a bent auxiliary outlet. The distinctive feature that makes this approach different from other types of passive capillary valves is the strong control of liquid movement, which is achieved by employing two adjustable sequential burst valves called a primary valve and a secondary burst valve. The guiding method can be used to route samples and reagents at given flow rates to a selection of receiving reservoirs, which are determined by the spinning frequency of the disc. The technique also allows for the switching of the flow direction instantaneously from the direction along the disc rotation to the opposite direction by increasing the rotational speed of the disc rather than relying on the Coriolis force, which would require reversing the spin direction. The flow routing by the proposed technique has been studied theoretically, and the flow behavior has been numerically investigated. These studies have been experimentally validated for a wide range of capillary sizes and for various liquids including di-water, mixtures of water and ethanol and bovine serum albumin (BSA).

Received 12th November 2014
Accepted 17th December 2014

DOI: 10.1039/c4ra14397c

www.rsc.org/advances

1 Introduction

Current standard clinical assays, such as enzyme-linked immunosorbent assays (ELISAs), often require expensive and bulky equipment, as well as skilful operators, for achieving reliable results. Such tests are mostly conducted in central lab facilities, which increases health care costs, delays the availability of results and is inconvenient for providing quality health care to underprivileged populations in remote rural areas, especially in developing countries.[1–3] In order to facilitate access to fast, inexpensive, and ubiquitous diagnostics, Lab-on-a-Chip (LOC) devices are attracting more and more attention as possible solutions for the automation of complex clinical and chemical processes. Compared to standard lab assays, LOCs come in a portable desktop form comparable or lower in cost than their larger counterparts, feature reduced time-to-results, require smaller amounts of sample and reagents and offer an increased possibility for multiplexing (simultaneous running of multiple tests from the same sample).[3–6] Currently, many of the steps in chemical and clinical assays, such as sample preparation (including blood serum separation and cell lysis, *etc.*),[7–10] DNA amplification (*e.g.*, with PCR) and the detection of nucleic acid targets,[11,12] are being developed on LOC devices, and some platforms have even attempted an integrated sample-to-answer solution.[13–15] Centrifugal microfluidics are a special type of realisation of the LOC concept on a spinning platform (typically in a geometric shape of a compact disc-CD) that contain chambers for samples, reagents and waste connected through a network of microchannels. On such a Centrifugal microfluidics, reagents/samples are propelled by the centrifugal force of the spinning disc to travel radially toward the outer edge of the disc. Various assay operations, including cell lysis, sample and analytical reagent mixing,[16,17] flow rate control,[18] volume definition and valving,[19–21] have been developed on Centrifugal microfluidics, and the technology is now considered mature enough for deployment in certain applications, such as disease detection and screening and drug testing.[4,22–29] A variety of flow control methods, including passive valves (requiring no external power sources) and active valves (requiring peripheral devices, such as a compressed air cylinder, heat guns or lasers),

[a]Department of Mechanical Engineering, Faculty of Engineering, University of Malaya, 50603, Kuala Lumpur, Malaysia. E-mail: kewmars.k.zad@gmail.com
[b]Department of Biomedical Engineering, Faculty of Engineering, University of Malaya, 50603, Kuala Lumpur, Malaysia
[c]Center for Innovation in Medical Engineering, Faculty of Engineering, University of Malaya, Kuala Lumpur, 50603, Malaysia
[d]Department of Biomedical Engineering, University of California, Irvine, 92697, USA. E-mail: fatimah@um.edu.my
[e]Department of Mechanical and Aerospace Engineering, University of California, Irvine, 92697, USA

† Electronic supplementary information (ESI) available. See DOI: 10.1039/c4ra14397c

are necessary for implementing complex assays on spinning platforms.[1,30–34] In most passive valves (*e.g.*, capillary valves, syphon valves, Coriolis valves, *etc.*), the valve actuation is mostly controlled by the angular velocity and the spinning direction of the disc.[30,35–37] Capillary valves that incorporate an abrupt geometrical change of the microchannel's cross-section are the most popular passive valves due to their simplicity and low cost of fabrication.[1,38–40] Capillary valves can stop liquid flow but only while the angular velocity does not exceed a critical rotation speed, *i.e.*, the burst frequency that depends on the properties of the fluid, the material of the channel walls, the distance of the capillary valve from the disc center and the geometric dimensions of the microchannel, including the angle of an expansion or contraction in the microchannel cross-section. It is at the burst frequency that the centrifugal pressure overcomes the capillary barrier pressure. A commercially successful example of a capillary valve, used in the Gyrolab Bioaffy CD, is based on a hydrophobic barrier that is patterned in a short section of a microchannel.[41,42] A technique was also proposed to change a channel surface from hydrophobic to hydrophilic by introducing chemical reagents into the fluid, thus allowing for a time-dependent opening of a valve.[43] A recent study demonstrated an LOC device constructed from polyester transparent sheets patterned with toner printed by a laser printer. The toner has a much higher surface contact angle than the surrounding polyester material, allowing the formation of capillary valves.[20] In complex assays where more precise control of the flow rate is required, other types of passive valves have been implemented, such as one based on elastic films that block flow in a microchannel and deflect in response to the centrifugal pressure.[21]

One of the major obstacles in efficient use of real-estate on the disc and thus in implementing complex multi-step assays on rotational microfluidic platforms is the need to overcome the unidirectionality of the flow. In general, the centrifugal and the fictitious Coriolis force determine the flow direction in microchannels and at T-junctions. Several methods have been introduced for propelling liquid against both the centrifugal force[1,30,32,44–47] and the Coriolis force.[48–51] The Coriolis force determines the movement of a liquid when it reaches a T-junction (a point where a channel splits into two channels). By exploiting the Coriolis force,[50] fluid at a T-junction can be switched to flow in either one of the channels or through both exit channels simultaneously (at low rotational frequencies). The flow switch in this method is based on the direction of the Coriolis force at high rotational frequencies that is dependent on the direction of the disc rotation; the reversal of the direction of rotation is needed to change the flow direction at T junctions. A liquid can also be routed first into one branching channel and then into a different branching channel when asymmetrical channels and chamber geometries are used. When the liquid filling a first chamber rises to a level that prevents the connection of the air in the branching channel with the vent hole in the first reservoir, the fluid in the main channel will be routed to a second reservoir.[51] Because the flow switch is based on the air trapped in the system it is incapable of switching the flow direction between exit channels more than once. More recently, an active flow switch method employing a periodically activated air supply was proposed to allow changing the flow direction without altering the direction of disc rotation.[49]

This paper introduces a novel approach to control the direction of flow at T-junctions on centrifugal microfluidic platforms that does not require the reversal of the spinning direction or external actuation sources and allows for non-stoppable flow switch between exit channels/chambers at T-junctions. We call our approach guided routing (GR); it allows for controlling the direction of the flow by changing only the rotational speed of the disc. For example, for a disc rotating clockwise, by increasing the rotational speed of the disc, the fluid flow changes direction from clockwise to counter-clockwise and *vice versa*. The mechanism of the new valve have been theoretically, experimentally and numerically studied. The volume of fluid (VOF) method of ANSYS-Fluent software was used to simulate the flow behavior in GR and the proposed mechanism is experimentally tested for various liquids.

2 Concept

Capillary valves on a centrifugal microfluidics prevent liquid from flowing as long as the rotational speed (rpm) is below a speed corresponding to a critical burst frequency; above that critical speed the flow rate and direction is based on the magnitude of the centrifugal and Coriolis forces. In order to improve the control over flow direction on a Centrifugal microfluidics, we introduce a new technique that does not require changing the spinning direction of the platform, applying surface treatments and/or employing external forces. This new passive flow control technique, which we call GR, relies on a two-stage valve comprised of (i) an auxiliary inlet, which is a recess that overlaps the capillary and the chamber it feeds into, and (ii) a bent auxiliary outlet, which is an extension of the auxiliary inlet recess, leading into the chamber as seen in Fig. 1. The first capillary valve that advancing fluid encounters is located at the junction of the capillary and the recessed auxiliary inlet and that valve will burst when the rotational frequency of the disc exceeds a primary burst frequency (ω_p). The second capillary valve is formed at the junction of the recessed auxiliary outlet and the chamber and it will burst when the rotational speed of the disc exceeds a secondary burst frequency (ω_s). By adjusting the spinning frequency of the disc after the primary burst frequency has been breached one can control the direction of the secondary burst that occurs when liquid flows into the chamber through the auxiliary outlet. When ω_p is smaller than ω_s, the fluid meniscus remains pinned at the auxiliary inlet/chamber interface while the fluid can advance in the auxiliary outlet and be guided by the bend of that outlet. When ω_p is larger than ω_s or when the angular velocity exceeds both ω_p and ω_s, the fluid will not stop at the auxiliary inlet/chamber interface and will flow into the chamber. The relative relationship between the primary and the secondary burst frequencies is determined by the materials selection and geometries of the chamber and channels of the described fluidic network. Fig. 1 illustrates the mechanism of GR in controlling the direction of flow in centrifugal microfluidic platforms. The flow behavior in

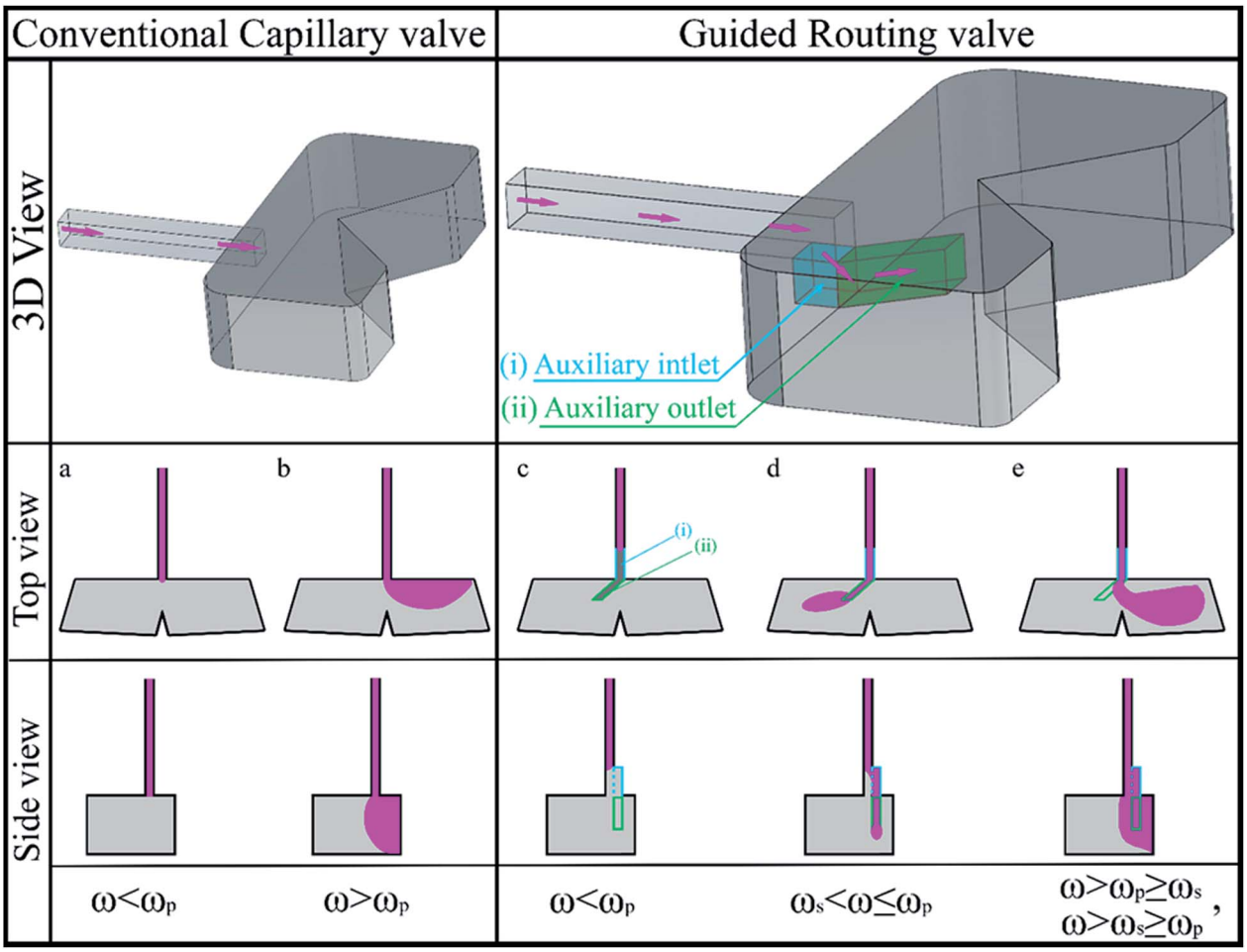

Fig. 1 A sketch of 3D, top and side views of a conventional capillary and a GR valve. In a GR valve, the liquid flow is controlled by confining the liquid stream temporarily into a specifically designed guided routing (GR) structure, which is comprised of two sections: an (i) auxiliary inlet and (ii) auxiliary outlet. In panels (a) and (b) (top view and side view), we show a traditional capillary valve on a centrifugal microfluidic platform that in panel (a) rotates clockwise with a spinning speed (ω) below its burst frequency (ω_p) and the liquid is pinned at the interface and in panel (b) as the platform rotates at a spinning speed above ω_p (where the Coriolis force is the predominant force) the liquid flows towards the Coriolis force. Panels (c) to (e) illustrate what happens in the case of a GR valve again with the platform rotating clockwise. In panel (c), the spinning speed is below the primary frequency ($\omega < \omega_p$) and the liquid is pinned at the auxiliary inlet. In panel (d), the platform rotates at a spinning speed above the secondary burst frequency and below or equal to the primary burst frequency and the liquid is guided by the auxiliary outlet. In panel (e), the liquid is routed towards the direction of the Coriolis force in two manners: (a) spinning the platform with a speed above the primary burst frequency if ω_p is larger or equal to the ω_s, and (b) spinning the platform with a speed above the secondary burst frequency if ω_s is larger or equal to the ω_s.

GR capillaries with different geometries corresponding to a wide range of rotational frequencies is investigated and discussed in the Results section below.

3 Materials and methods

3.1 Experimental setup

The centrifugal microfluidic platforms with the GR valves were fabricated using a Computer Numerical Control (CNC) machine *i.e.*, model VISION 2525, by Vision Engraving and Routing Systems, USA. The experiments were conducted on a custom-made system consisting of a digital disc spin test system, laser sensor and a high-speed camera (see Fig. 2). Microstructures were milled in three 2 mm thick polymethyl methacrylate (PMMA) layers that were bonded together with two 0.056 mm thick pressure sensitive adhesive (PSA) layers (by FLEXcon, USA). Fig. 3 shows an exploded view of the thus assembled five layer CD-like device used in the current study. The first substrate containing vent holes is bonded to the middle substrate containing microchannels, inlet and outlet chambers. The guided routing valves are milled on the lowest layer and bonded to the middle substrate layer. The microstructures formed in the PSA layers conforming to the designs in the PMMA layer are cut by a cutter plotter (model PUMA II, by GCC, Taiwan).

3.2 Theory

Apart from the use of hydrophobic patches, liquid routing in most passive techniques depends on the direction of the disc rotation and the ratio of the centrifugal to the Coriolis force. In

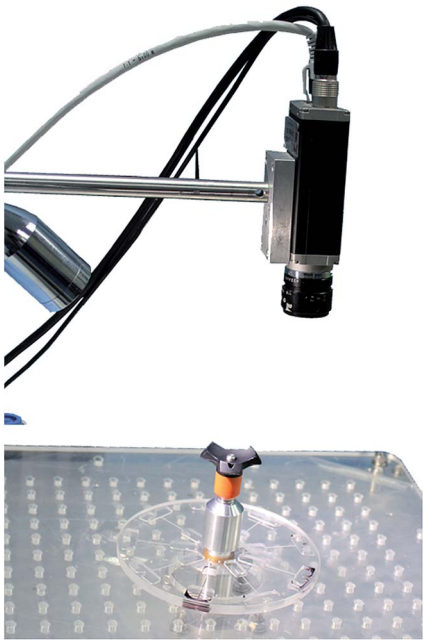

Fig. 2 The custom-made experimental setup.

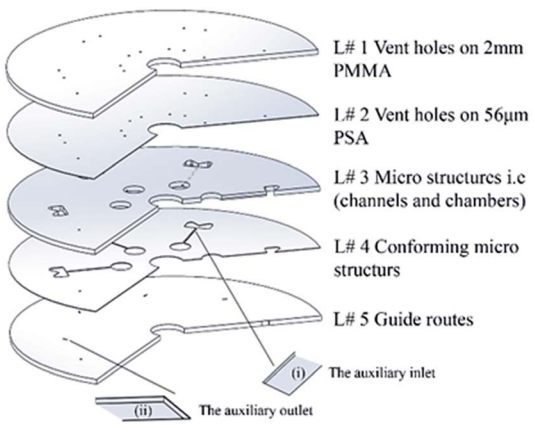

Fig. 3 An exploded view of the disc assembly. Guided routing valves (GR) are located on the fourth and fifth layers of the assembled disc.

addition to these parameters, Kazemzadeh *et al.*[52] have shown the effect of an asymmetric expansion of a capillary channel on the liquid flow direction and on the performance of the capillary valves. The present technique relies on a balance between the centrifugal and Coriolis forces and the distinctive capillary pressures at the GR valve. The valving technique benefits from two adjustable sequential bursts: a primary and secondary burst occurring at the auxiliary inlet and the auxiliary outlet, respectively. The body forces applied to fluidic elements on a rotating reference frame include the sum of total pressure and viscous forces (see Fig. 4). For a non-inertial, incompressible system, the Navier–Stokes equations are:[53]

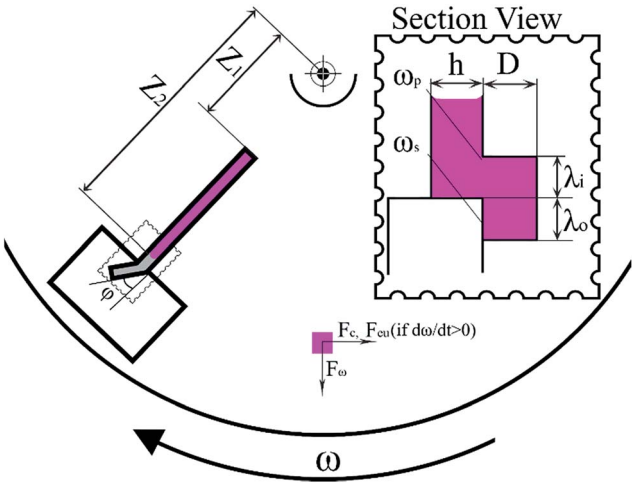

Fig. 4 Partial view of a disc spinning at ω containing a GR valve with an auxiliary inlet and outlet length of λ_i and λ_o, respectively, and a liquid plug exposed to radial centrifugal and transversal Coriolis force.

$$\sum F_x = -F_{co} + \mu\left(\frac{\partial^2 v_x}{\partial x^2} + \frac{\partial^2 v_x}{\partial y^2} + \frac{\partial^2 v_x}{\partial z^2}\right) = \rho\left(\frac{\partial v_x}{\partial t} + v_x\frac{\partial v_x}{\partial x} + v_y\frac{\partial v_y}{\partial y} + v_z\frac{\partial v_z}{\partial z}\right) \quad (1a)$$

$$\sum F_z = -F_\omega + \mu\left(\frac{\partial^2 v_z}{\partial x^2} + \frac{\partial^2 v_z}{\partial y^2} + \frac{\partial^2 v_z}{\partial z^2}\right) = \rho\left(\frac{\partial v_z}{\partial t} + v_x\frac{\partial v_z}{\partial x} + v_y\frac{\partial v_z}{\partial y} + v_z\frac{\partial v_z}{\partial z}\right) \quad (1b)$$

where ρ, $a_{x,z}$, μ, and $v_{x,z}$ are density, acceleration in the x and z directions, viscosity and velocity in the x and z directions, respectively. The forces per unit volume in x and z direction are due to the vector product of Coriolis and centrifugal accelerations, respectively. The centrifugal force per unit volume is given as:

$$F_\omega = \frac{\rho\omega^2}{\Delta r}\int_{r_1}^{r_2} r\mathrm{d}r = \frac{\rho\omega^2}{2\Delta r}\left({r_2}^2 - {r_1}^2\right) = \frac{\rho\omega^2}{2\Delta r}(r_2 - r_1)((r_2 + r_1) = \rho\omega^2\bar{r}$$

$$\bar{r} = \frac{r_1 + r_2}{2} \quad (2)$$

where ω is the spinning frequency of the disc, r_1 and r_2 are the inner and outer radial position of a liquid plug, and $\bar{r}$ is the mean radial position of the liquid. The primary burst frequency of a GR valve, similar to the burst frequency of a regular capillary valve, can be obtained from the Young–Laplace equation. However, the specific geometry of a GR valve features two contact angles (θ_1 on the bottom surface and θ_2 on the top surface of the valve structure) that change dynamically as a function of the length of the auxiliary inlet and the centrifugal pressure (see Fig. 5a). In order to cause the liquid to flow in the auxiliary inlet before it reaches the expansion, the advancing contact angle of the bulged meniscus θ_2 must be higher than $\theta_1 - 90°$. The optimum value of θ_2 occurs when the length of the auxiliary inlet λ_i is equal to the channel height, which is when

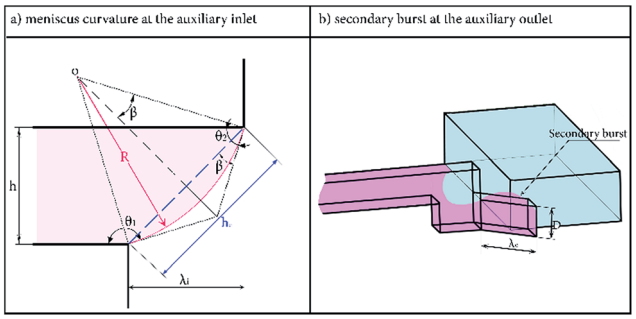

Fig. 5 The burst frequencies of a GR valve: (a) a primary burst occurring at the auxiliary inlet when λ_i is equal to the microchannel height, (b) a secondary burst at the auxiliary outlet.

$\theta_2 = \theta_1 + 90°$. In these circumstances the liquid will flow into the auxiliary inlet instead of flowing along the top surface of it and will avoid the unfavorable valve burst, which occurs when the liquid continues to flow along the top surface of the auxiliary outlet (when $\theta_2 > \theta_1 - 90)°$. Fig. 5 demonstrates that when $\lambda_i = h$ the primary burst pressure can be predicted based on Laplace equation:[54]

$$\Delta P_b = 2\sigma_{la}\left(\frac{\cos(\theta+\beta)}{h_e} + \frac{\cos\theta}{w}\right) \quad (3)$$

where, σ_{la}, θ, β, w and h_e are liquid surface tension, the contact angle, the channel width and the expansion angle and effective height of microchannel, respectively (see Fig. 5a). It can be gleaned from Fig. 5b that the secondary burst in a GR valve occurs when the liquid is released from the recessed area of the auxiliary outlet and can be calculated from equations presented earlier in other studies.[55,56] In order to determine the flow direction based on the spinning frequency of the disk, the maximum radial velocity is required to determine the dominant force acting on the liquid at the GR junction. The maximum radial velocity is found by writing the Navier–Stokes equation in the plane parallel to the disc surface. Typically, the gravitational force is significantly smaller than other forces on a spinning disc and thus can be ignored. We also assume fluid of constant density and because the walls are impermeable, the liquid is confined to flow in the z direction and there are no changes of the fluid velocity except in the direction of the flow:

$$-\rho\omega^2\bar{r} + \mu\left(\frac{\partial^2 v_z}{\partial x^2} + \frac{\partial^2 v_z}{\partial x^2}\right) = \rho\left(v_z\frac{\partial v_z}{\partial z}\right) \quad (4)$$

Now, considering that the flow is fully developed, the velocity of the fluid in the direction of the flow is constant and due to the no-slip condition at the wall, $v_z = 0$ at $x = 0$ and $x = w$. Therefore, the maximum velocity is at $x = 0.5w$ and it is equal to:

$$v_z = \frac{\rho\omega^2\bar{r}}{8\mu}w^2 \quad (5)$$

The ratio of Coriolis to centrifugal force is then given by:

$$\frac{F_{co}}{F_\omega} = \frac{\rho\omega w^2}{4\mu} \quad (6)$$

The liquid flows in the direction of the Coriolis force if, $\frac{F_{co}}{F_\omega} \gg 1$,[50] therefore increasing the spinning frequency to meet that condition makes it possible for the liquid to flow in the direction of the Coriolis force without having to reverse the spinning direction of the disc. In addition, the Euler force $F_{Eu} = -\rho\alpha \times r$ assists in instantaneous switching of the flow direction from the direction of the auxiliary outlet to the opposite direction when $\frac{F_{Eu}}{F_\omega} \gg 1$.

3.3 Numerical analysis

The volume of fluid (VOF) method from the commercial ANSYS-Fluent CFD package, version 13.1, was used to simulate the flow behavior within the fluidic network under study. The details of the method and formulations of the numerical analysis are given in our previous studies in Kazemzadeh *et al.*[52,57] Briefly, the computational domain was set to rotate clockwise with an initial rotational frequency of 50 rpm, which was increased in steps of 50 rpm. Zero fluid velocity is set at all the walls of the microstructures (in accordance with the no-slip boundary condition). In order to consider the effects of surface tension, centrifugal and Coriolis forces, the body-force-weighted interpolation scheme was used in the numerical calculation. The scaled residuals were set at 1×10^{-6} as the convergence criterion for the continuity and other governing equations. The area adjacent to the GR was simulated using a uniform quad grid and the accuracy of the simulation results was evaluated by comparing the numerical with our experimental data and theoretical analyses.

4 Results and discussion

4.1 Flow behavior

Capillary valves are typically fabricated by either a one- or two-dimensional expansion in microchannels due to their ease of fabrication (see Fig. 6). The difference between the commonly used capillaries (two dimensional) and GR valves is that in the commonly used capillaries the meniscus is pinned in the plane perpendicular to the disc surface, holding its convex shape at the expansion point, and the meniscus expands on the surfaces of the outlet chambers (for more details on conventional capillaries refer to ref. 56 and 57). In a GR valve, on the other hand, the meniscus expands in the perpendicular plane and simultaneously advances in the parallel plane, retaining its convex shape. In comparison with a conventional capillary valve, a GR valve generates an either slightly weaker or a slightly stronger blockage to the flow, depending on the capillary width (*i.e.*, due to the effect of the channel aspect ratio on the burst pressure, studied in ref. 55, 57 and 58). However, this difference can often be neglected in designing sequential operations because the interval between the burst frequencies in sequential processes on a Centrifugal microfluidics is kept at

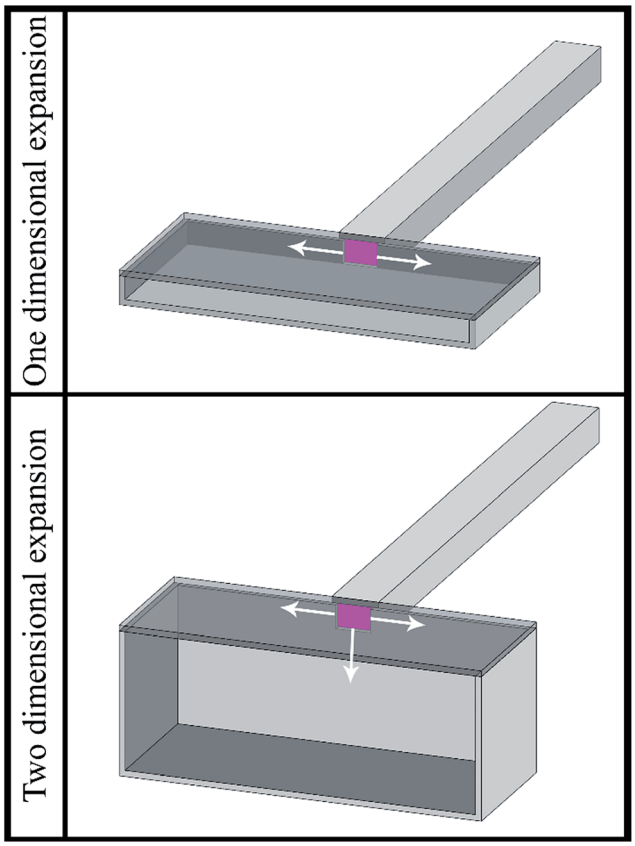

Fig. 6 Three-dimensional view of the possible methods of fabricating capillary valves.

approximately 200 rpm to avoid unwanted release of samples/reagents.[58] Fig. 7 shows the sequential movement of the liquid adjacent to a GR valve and the outlet chamber where the rotational frequency is gradually increased to the burst frequency of the valve. The maximum distance that the meniscus is able to expand in the radial direction (x_m) before the valve bursts into the auxiliary inlet is proportional to the height of the capillary. The radial length that the meniscus can expand before reaching the outlet chamber is proportional to the groove height and the capillary height. Fig. 7a–c show that while the liquid meniscus is pinned at the top surface of a GR valve, the meniscus continues its expansion from the bottom surface and flows into the auxiliary inlet and later into the auxiliary outlet.

4.2 Characterization

The mechanism of the GR valve is characterised by experimentally and numerically investigating the influence of λ_i and λ_o on the burst frequency when employing different liquids (where λ_i and λ_o are the length of the auxiliary inlet and the auxiliary outlet, respectively (see Fig. 4). The optimum lengths of the auxiliary inlet (λ_i) and the auxiliary outlet (λ_o) are defined by constructing several GRs with different λ_i and λ_o. The minimum λ_i and λ_o are equal to $h/2$ and are increased in a step size of 0.1 mm. The effect of surface tension and protein absorbance on the GR valve operation is investigated by conducting several experiments using different liquids, such as deionised water, a mixture of ethanol and water, and with bovine serum albumin (BSA). A comparison of burst

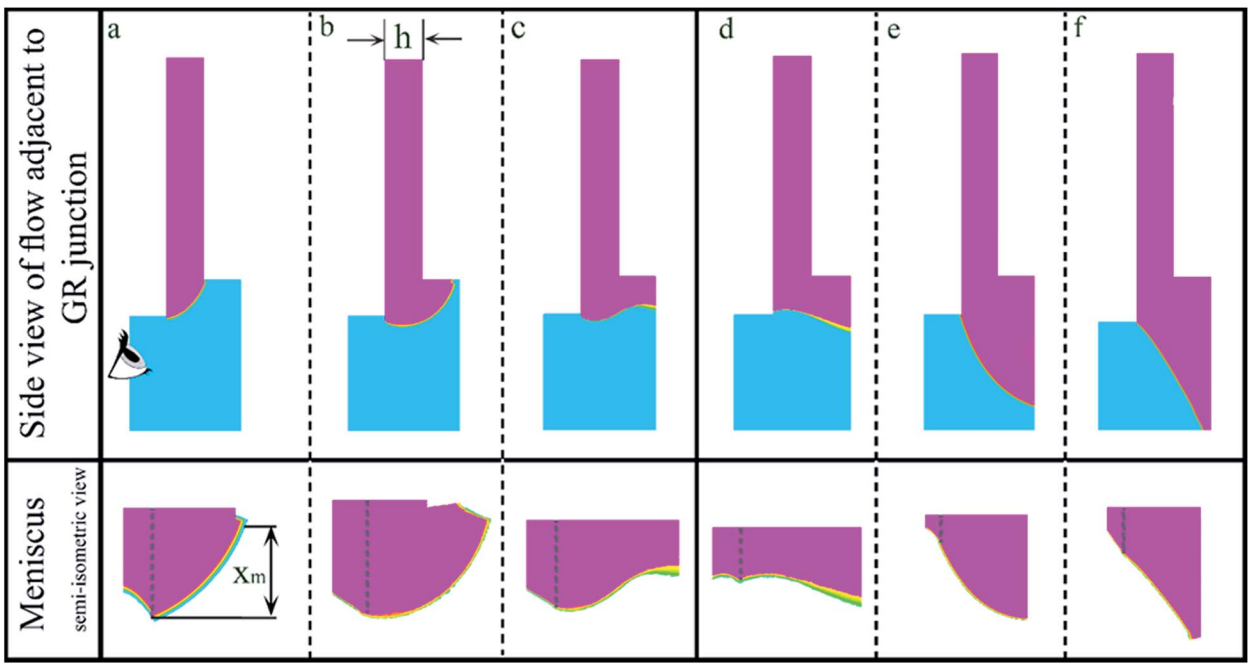

Fig. 7 Numerically obtained sequential images of meniscus advancement in response to increasing the rotational frequency for a capillary of 200 × 200 μm and a GR with an auxiliary inlet and outlet of 200 μm. The meniscus experiences a two-dimensional motion due to the geometrical condition of the capillary. As the rotational frequency is gradually increased and liquid reaches the GR expansion, the meniscus continues its radial advancement along the capillary with its initial convex shape; however, the meniscus expands in the perpendicular direction to the disc surface (a). The first burst of the GR valve occurs (b) and after that a fluctuating movement of the meniscus is observed and the portion of meniscus previously advanced is pulled back due to the advancement of the portion of meniscus previously pinned (c and d). By increasing the rotational speed, the liquid will flow in the groove (e and f).

Table 1 The effect of GR on the burst frequency (f_b) for different liquids at $\bar{r} = 39$ mm and capillary channels with the same height (h) and width (w) of 200 and 400 μm

Substance	$w = h$ (μm)	λ_i (mm)	λ_2 (mm)	Num. f_b[a] (rpm)	Exp. f_b[b] (∼rpm)
Deionised water	200	0	0	450–500	480
		0.2	0.1, 0.2, 0.3	450–500	450–460
		0.3	0.2, 0.3, 0.4	300–350	340
	400	0	0	150–200	190
		0.4	0.3, 0.4, 0.5	150–200	160–170
		0.6	0.5, 0.6, 0.7	100–150	120–130
BSA	200	0	0	400–450	410–420
		0.2	0.1, 0.2, 0.3	350–400	380
		0.3	0.2, 0.3, 0.4	250–300	300
	400	0	0	150–200	140–150
		0.4	0.4, 0.5, 0.6	100–150	110
		0.6	0.5, 0.6, 0.7	100–150	100

[a] The numerical rotational speed was increased in steps of 50 rpm. [b] Values after conducting several experiments.

frequencies of deionised water and BSA in normal capillaries and capillaries equipped with GRs is compiled in Table 1. The table shows the effect that λ_i and λ_o have on the burst frequency of GR valves with cross sections of 200 × 200 μm and 400 × 400 μm. The burst frequency reduces dramatically when $x_c > h$, which can be explained by the manner in which the meniscus advances. When $x_c \neq h$, the meniscus advances along the top surface until it is pinned at the incline where a higher centrifugal pressure is required to continue the advance of the liquid front. The increase in the length of the groove ($x_c > h$) facilitates a smooth advancement of the liquid meniscus on the top surface until θ_1 reaches 180° and the GR valve bursts. At $x_m \approx h$, the meniscus is pinned at the top surface with the contact angle θ_2 much lower than the angle required for bursting, while at the bottom the contact angle θ_1 is at the threshold to burst.

5 Applications

5.1 Flow switch

In many types of microfluidic functions, such as separation and other preparative protocols, separated samples, such as washing and elution buffers, are required to be directed to the waste or other receiving chambers. For example, it is often required to separate red blood cell and plasma and guide them into different outlet chambers. It can also be also used in mixing different liquids by splitting and recombination of the liquid. Several techniques (*e.g.*, Coriolis-based strategies or hydrophobic patches) have been pursued for routing a sequence of distinct volumes to designated vessels as a common task in preparative protocols or more specific assignments on intricate assays in Centrifugal microfluidics systems.[20,23] As a demonstration for one of the many possible applications, different microchannels equipped with GR valves were fabricated in order to control the flow direction on a spinning microfluidic disc that contains inlet and outlet chambers connected *via* a fluidic network of microchannels. The GR flow switching experiments are conducted for various sizes of microchannels, GR dimensions, and types of liquids. The height and the length of GRs vary from 0.5h to 2h, where h is the height of the capillary. The width of the grooves is kept identical to the width of the corresponding capillary microchannel on the same disc. Black-dyed deionised water is dispensed into the inlet chamber of a GR capillary and the experiment commences by spinning the disc and gradually increasing the angular velocity in 10 rpm increments until the capillary valve bursts. Fig. 8 shows that the liquid can be direct entirely into one of the outlet chambers at low and into the other one at high frequencies. It also shows the ability of the valve to continuously change the flow direction from one to another outlet chamber by reducing or increasing the rotational velocity. The figure shows the sequential movement of liquids in a capillary of $w = h = 400$ μm without and with a GR valve of $\lambda_i = \lambda_o = 400$ μm (these terms are explained in Fig. 1). Fig. 8a and b shows the sequences of liquid movement before the first and second burst frequencies of a GR valve. The gradual increase of the spinning frequency up to ∼170 rpm causes the liquid to flow in the direction of the auxiliary outlet (Fig. 8c and d). The liquid continues to flow in the direction of the microchannel, because of the momentary relation between the centrifugal and the Coriolis force (*i.e.*, it is similar to liquid movement at low rotational frequencies after bursting into the chamber in conventional microchannels). The abrupt increment in the spinning frequency (to 370 rpm) causes the liquid to detour from the tip of the route channel toward the direction of the Coriolis forces (Fig. 8e and f). At any moment after the abrupt increase in spinning frequency, a reduction of the spinning frequency to its previous value will cause the liquid to flow along the auxiliary outlet and towards its previous direction (the ESI† Video is available in the supplementary section). The video shows that initially liquid flows in the direction of disc rotation and by increasing the rotational frequency it flows in the opposite direction; and consequently the liquid flow switches back to its previous direction by reduction of the rotational frequency. For the current capillary dimension and $\bar{r} = 39$ mm, the flow is switched to the direction of Coriolis at ∼350 rpm and in the direction of the auxiliary outlet at ∼170 rpm. The performance of the GR valve under continuous operation was investigated for several liquids and the results show that all the liquids were successfully guided by the GR valve. The

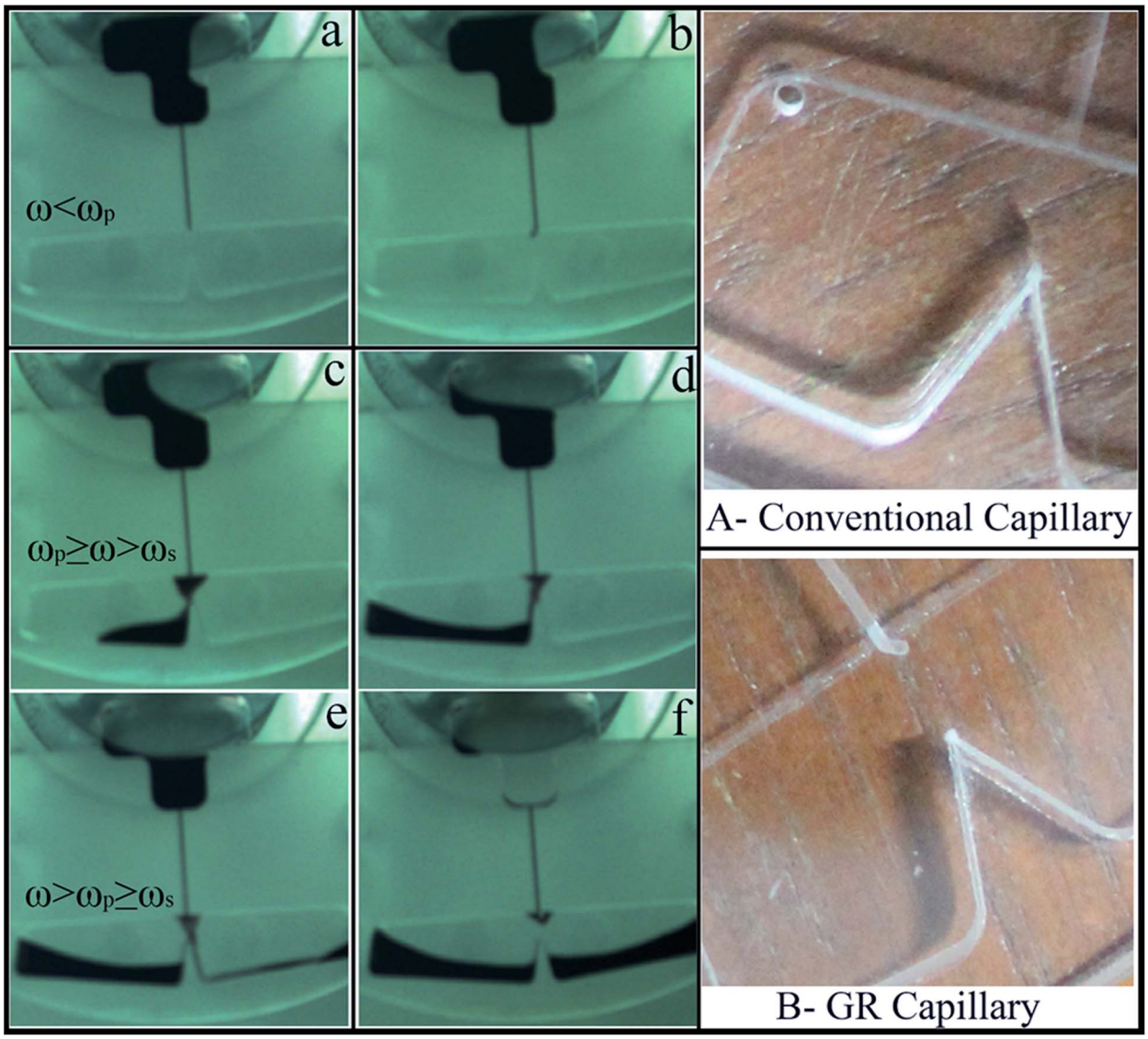

Fig. 8 Partial top view of the liquid motion in a GR-equipped capillary in a clockwise rotating disc. The height and width of the capillary both are 400 μm; the length of GR valve along the capillary (auxiliary inlet) λ_i is 400 μm; the length of the segment sloped in the direction of disc rotation (auxiliary outlet) λ_o is 600 μm.

effect of protein adsorption on the PMMA surfaces, which occurs in most of the clinical assays where biological substances are used, was investigated by conducting the experiments using BSA. The consecutive loading and emptying of the same microstructure up to 5 times with 10 minute intervals between each experiment shows up to 50–60 rpm reduction of the initial burst frequency. Note that the switching frequency is independent of the burst frequency of the capillary valve because the GR controls the fluid flow after bursting. The experimental observations presented in Table 2 shows that a minimum value of the auxiliary outlet for successfully switching the flow direction is equal to the height of the channel; however, $\lambda_o > h$ will guarantee a consistent control of the liquid flow in the direction of the auxiliary outlet. It confirm that the optimum length of the auxiliary inlet is $\lambda_i = h$ and that for $\lambda_i > h$ the GR valve is unable to take control of the flow.

Table 2 The response of flow to the auxiliary inlet and outlet dimensions and experimental flow switch frequencies

H (μm)	λ_i (μm)	λ_o (μm)	F (rpm)	F (rpm)	C.W.	C.C.W.
200	>200	</>200	≲420	>700	x^b	$\surd^a$
	~200	≥200	≲460		$\surd$	$\surd$
400	>400	</>400	≲150	>370	x	$\surd$
	~400	≥400	≲170		$\surd$	$\surd$
700	>700	</>700	≲110	>350	x	$\surd$
	~700	≥700	≲140		$\surd$	$\surd$

[a] Successful flow switch. [b] Unsuccessful flow switch.

5.2 Fluid distribution

As a demonstration of another application of GR valving, we describe the function of a GR valve for dividing a liquid flow into several side streams with a given flow rate above the burst

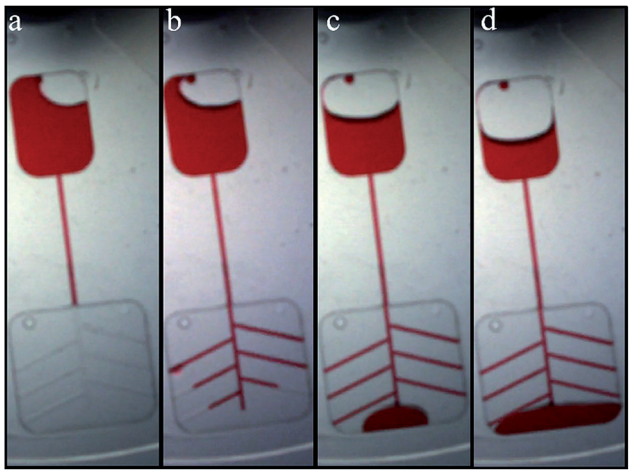

Fig. 9 A sequence of photographs of the rotating disc demonstrating the routing of the liquid by using GR valve.

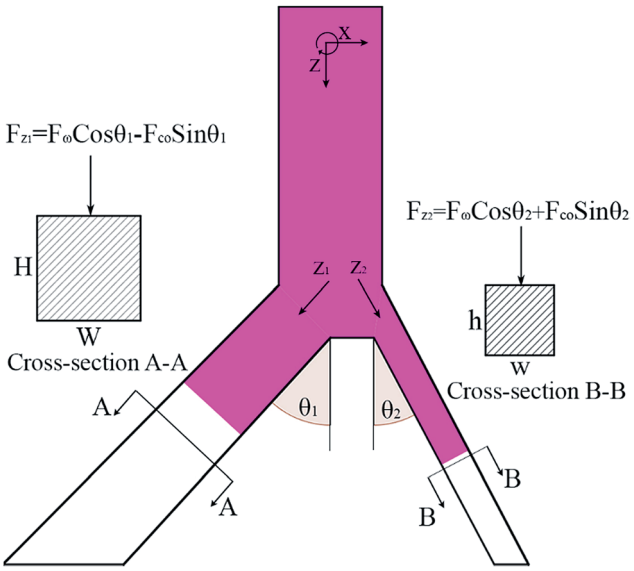

Fig. 10 Free body diagram of a GR with two branch channels splitting at a junction.

without applying surface treatments or employing external power sources. The capability of a GR valve for flow control and distribution of the liquid is investigated by conducting a simple experiment wherein the auxiliary inlet of a GR valve is connected to several outlet branches with the same dimensions engraved in the outlet chamber. Fig. 9 shows a microfluidic structure consisting of an inlet and an outlet chamber connected by a GR capillary. The inlet chamber is loaded with red-dyed deionised water and the experiment commences by spinning the disc until the GR valve bursts. As can be gleaned from Fig. 9 as a consequence of using a GR, after the secondary burst of the valve, the liquid flows into the designated paths. This capability of a GR valve can be employed to regulate and distribute liquids with different flow rates in different directions.

Fig. 10 shows the free body diagram of a GR with two branch channels splitting at a junction. At the point where the main channel meets two branch channels, the overall propelling force can be written as components of the centrifugal and Coriolis forces in the direction of the branching outlet channels (as indicated in Fig. 10):

$$F_{z_1} = F_\omega \cos\theta_1 - F_{co} \sin\theta_1$$
$$F_{z_2} = F_\omega \cos\theta_2 - F_{co} \sin\theta_2 \quad (7)$$

where F_{z_1} and F_{z_2} are total propelling forces in the direction of each outlet branch. The splitting of the incoming fluid between two outlet branches of equal hydraulic diameters is regulated by the ratio of the forces:

$$\frac{\sum F_{z_1}}{\sum F_{z_2}} = k \quad (8)$$

The flow will be equally divided into two outlet branches when $k = 1$. The equal division of the liquid into two streams can be used to reduce the consumption of samples by duplicating the detection chambers, for example in the CD-like-ELISA chips.[58,59] Substituting eqn (7) in eqn (8), the difference between angles of two outlet branches is:

$$\Delta\theta = 2\tan^{-1}\left(\frac{\rho\omega w^2}{4\mu}\right) \quad (9)$$

where θ_1 and θ_2 are the separation angle against the direction and in the direction of Coriolis force. In addition, as the flow in most of the microfluidic platforms is laminar, the branch channel dimensions can be employed to manipulate the flow resistance and regulate the flow distribution to each branch.[60] Poiseuille's law can be rewritten in terms of the flow rate:[61]

$$Q = \Delta P \frac{D_h{}^2 A}{32\mu L} = \frac{\Delta P}{R} \quad (10)$$

where L, D_h, A, V and R are the branch channel length, the hydraulic diameter, the cross sectional area of the channel, the velocity and the resistance to flow, respectively:

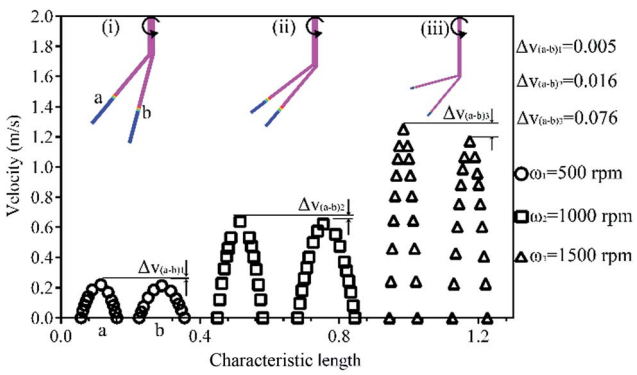

Fig. 11 Numerically obtained velocity magnitudes in branch channels (a and b) bifurcated evenly from the capillary of 200 × 200 μm. The branch channels are simulated according the angle calculated from eqn (9), where $\theta_1 = 40°$.

$$R = \frac{32\mu L}{D_h{}^2 A} \quad (11)$$

Thus, for a fluid of uniform viscosity and channels of given dimensions, the flow rate for the splitting branches can be calculated. In order for the parabolic velocity profile to develop completely within the branching channels, the length of the auxiliary outlet λ_o (see Fig. 1) has to be greater than entrance length (l_e) of:[61]

$$\lambda_o > l_e = 0.035 D_h \mathrm{Re} \quad (12)$$

The accuracy of eqn (8) in predicting the flow rate in branch channels has been evaluated by carrying out several simulations according to the angles predicted based on eqn (9). Fig. 11 shows the velocity distribution in branch channels of a 200 × 200 μm GR spinning at rotational frequencies of (i) 500, (ii) 1000 and (iii) 1500 rpm and $\theta_1 = 40^\circ$. The figure shows that using the suggested separation angles (calculated by eqn (10)) enhances the accuracy of the uniform distribution of liquid for branch channels up to 99.5, 97.4 and 94% for the rotational frequency of 500, 1000 and 1500 rpm, respectively. The small difference between the velocities of branch channels at high rotational speed may be reduced by small geometrical changes at the point where branches are separated from the main channel. The equation can also be used to define different velocity rates at each branch channel by integrating it with flow resistance equation.

6 Conclusion

This paper introduces a novel technique called guided routing (GR) to control and manipulate the fluid flow after capillary valve bursting on a centrifugal microfluidic disc. The introduced method is capable of determining the direction of the flow in T-junctions as well as guiding the liquid into several branches. The experimental results show that GR is able to continuously switch the flow direction; the fluid flows in the direction of disc rotation at low rotational speeds and instantaneously changes to the opposite direction with an abrupt increase of the rotational speed. The capability of the valve to equally distribute the flow into two branches has been theoretically and numerically presented. This valving technique is applicable to clinical and chemical operations for which switching the flow direction or equal and non-equal dividing the liquid is required.

Acknowledgements

This research was supported by the University of Malaya (UM) High Impact Research Grant UM-MOHE UM.C/625/1/HIR/MOHE/05 from the Ministry of Higher Education Malaysia (MOHE) and University of Malaya Research Grant (UMRG RP009A-13AET). The authors would like to acknowledge Prof. Dr Noorsaadah Abd Rahman from Department of Chemistry, Faculty of Science, University of Malaya and her grant "Hits-to-Lead: Designing Dengue Virus Inhibitors, National Biotechnology Directorate (NBD) Initiative-Malaysian Institute of Pharmaceuticals and Nutraceuticals (IPharm), Ministry of Science, Technology and Innovation (MOSTI IPHARM 53-02-03-1049)" for partially sponsoring the initial setup of the CD Spin Test System. Fatimah Ibrahim would like to acknowledge the Yayasan Sultan Iskandar Johor Foundation for funding the one-off special equipment grant in this research. Marc Madou acknowledges support of the National Institutes of Health (Grant 1 R01 AI089541-01).

References

1 M. Madou, J. Zoval, G. Jia, H. Kido, J. Kim and N. Kim, *Annu. Rev. Biomed. Eng.*, 2006, **8**, 601–628.
2 J. V. Zoval and M. J. Madou, *Proc. IEEE*, 2004, **92**, 140–153.
3 B. S. Lee, J.-N. Lee, J.-M. Park, J.-G. Lee, S. Kim, Y.-K. Cho and C. Ko, *Lab Chip*, 2009, **9**, 1548–1555.
4 W. Lee, J. Jung, Y. K. Hahn, S. K. Kim, Y. Lee, J. Lee, T.-H. Lee, J.-Y. Park, H. Seo, J. N. Lee, J. H. Oh, Y.-S. Choi and S. S. Lee, *Analyst*, 2013, **138**, 2558–2566.
5 B. S. Lee, Y. U. Lee, H.-S. Kim, T.-H. Kim, J. Park, J.-G. Lee, J. Kim, H. Kim, W. G. Lee and Y.-K. Cho, *Lab Chip*, 2011, **11**, 70–78.
6 N. Godino, R. Gorkin III, A. V. Linares, R. Burger and J. Ducree, *Lab Chip*, 2013, **13**, 685–694.
7 L. Nan, Z. Jiang and X. Wei, *Lab Chip*, 2014, **14**, 1060–1073.
8 J. Reboud, Y. Bourquin, R. Wilson, G. S. Pall, M. Jiwaji, A. R. Pitt, A. Graham, A. P. Waters and J. M. Cooper, *Proc. Natl. Acad. Sci. U. S. A.*, 2012, **109**, 15162–15167.
9 X. Li, W. Chen, G. Liu, W. Lu and J. Fu, *Lab Chip*, 2014, **14**, 2565–2575.
10 J. Zhang, S. Yan, W. Li, G. Alici and N.-T. Nguyen, *RSC Adv.*, 2014, **4**, 33149–33159.
11 R. Jenison, H. Jaeckel, J. Klonoski, D. Latorra and J. Wiens, *Analyst*, 2014, **139**, 3763–3769.
12 S. Ma, D. N. Loufakis, Z. Cao, Y. Chang, L. E. K. Achenie and C. Lu, *Lab Chip*, 2014, **14**, 2905–2909.
13 M. Ritzi-Lehnert, R. Himmelreich, H. Attig, J. Claußen, R. Dahlke, G. Großhauser, E. Holzer, M. Jeziorski, E. Schaeffer, A. Wende, S. Werner, J. Wiborg, I. Wick, K. Drese and T. Rothmann, *Biomed. Microdevices*, 2011, **13**, 819–827.
14 S. Schumacher, J. Nestler, T. Otto, M. Wegener, E. Ehrentreich-Forster, D. Michel, K. Wunderlich, S. Palzer, K. Sohn, A. Weber, M. Burgard, A. Grzesiak, A. Teichert, A. Brandenburg, B. Koger, J. Albers, E. Nebling and F. F. Bier, *Lab Chip*, 2012, **12**, 464–473.
15 P. Song, R. Hu, D. J. H. Tng and K.-T. Yong, *RSC Adv.*, 2014, **4**, 11499–11511.
16 W. W.-F. Leung and Y. Ren, *Int. J. Heat Mass Transfer*, 2013, **64**, 457–467.
17 Y. Ren and W. W.-F. Leung, *Chem. Eng. J.*, 2013, **215–216**, 561–578.
18 A. P. Bouchard, D. A. Duford and E. D. Salin, *Anal. Chem.*, 2010, **82**, 8386–8389.
19 A. Kazarine and E. D. Salin, *Lab Chip*, 2014, **14**, 3572–3581.

20 Y. Ouyang, S. Wang, J. Li, P. S. Riehl, M. Begley and J. P. Landers, *Lab Chip*, 2013, **13**, 1762–1771.
21 H. Hwang, H.-H. Kim and Y.-K. Cho, *Lab Chip*, 2011, **11**, 1434–1436.
22 A. L. Brogger, D. Kwasny, F. G. Bosco, A. Silahtaroglu, Z. Tumer, A. Boisen and W. E. Svendsen, *Lab Chip*, 2012, **12**, 4628–4634.
23 O. Strohmeier, N. Marquart, D. Mark, G. Roth, R. Zengerle and F. von Stetten, *Anal. Methods*, 2014, **6**, 2038–2046.
24 O. Ymbern, N. Sandez, A. Calvo-Lopez, M. Puyol and J. Alonso-Chamarro, *Lab Chip*, 2014, **14**, 1014–1022.
25 G. Aguirre, V. Efremov, M. Kitsara and J. Ducrée, *Microfluid. Nanofluid.*, 2014, 1–14, DOI: 10.1007/s10404-014-1450-7.
26 J. Marchalot, Y. Fouillet and J.-L. Achard, *Microfluid. Nanofluid.*, 2014, **17**, 167–180.
27 M. M. Aeinehvand, F. Ibrahim, S. W. Harun, I. Djordjevic, S. Hosseini, H. A. Rothan, R. Yusof and M. J. Madou, *Biosens. Bioelectron.*, DOI: 10.1016/j.bios.2014.08.076
28 T. van Oordt, G. B. Stevens, S. K. Vashist, R. Zengerle and F. von Stetten, *RSC Adv.*, 2013, **3**, 22046–22052.
29 M. Czugala, D. Maher, F. Collins, R. Burger, F. Hopfgartner, Y. Yang, J. Zhaou, J. Ducree, A. Smeaton, K. J. Fraser, F. Benito-Lopez and D. Diamond, *RSC Adv.*, 2013, **3**, 15928–15938.
30 M. M. Aeinehvand, F. Ibrahim, S. W. Harun, W. Al-Faqheri, T. H. G. Thio, A. Kazemzadeh and M. Madou, *Lab Chip*, 2014, **14**, 988–997.
31 M. Amasia, M. Cozzens and M. J. Madou, *Sens. Actuators, B*, 2012, **161**, 1191–1197.
32 K. Abi-Samra, L. Clime, L. Kong, R. I. Gorkin, T. H. Kim, Y. K. Cho and M. Madou, *Microfluid. Nanofluid.*, 2011, **11**, 643–652.
33 M. J. Madou, L. J. Lee, S. Daunert, S. Lai and C.-H. Shih, *Biomed. Microdevices*, 2001, **3**, 245–254.
34 N. R. Glass, R. J. Shilton, P. P. Y. Chan, J. R. Friend and L. Y. Yeo, *Small*, 2012, **8**, 1881–1888.
35 R. Gorkin III, C. E. Nwankire, J. Gaughran, X. Zhang, G. G. Donohoe, M. Rook, R. O'Kennedy and J. Ducrée, *Lab Chip*, 2012, **12**, 2894–2902.
36 R. Gorkin, S. Soroori, W. Southard, L. Clime, T. Veres, H. Kido, L. Kulinsky and M. Madou, *Microfluid. Nanofluid.*, 2012, **12**, 345–354.
37 T.-H. Kim, H. Hwang, R. Gorkin, M. Madou and Y.-K. Cho, *Sens. Actuators, B*, 2013, **178**, 648–655.
38 C. Lu, Y. Xie, Y. Yang, M. M.-C. Cheng, C.-G. Koh, Y. Bai, L. J. Lee and Y.-J. Juang, *Anal. Chem.*, 2007, **79**, 994–1001.
39 T.-S. Leu and P.-Y. Chang, *Sens. Actuators, A*, 2004, **115**, 508–515.
40 P. F. Man, C. H. Mastrangelo, M. A. Burns and D. T. Burke, Microfabricated capillarity-driven stop valve and sample injector, *Proc. - IEEE Annu. Int. Workshop Micro Electro Mech. Syst., 11th*, 1998, 45–50.
41 http://www.gyros.com.
42 M. Inganäs, H. Dérand, A. Eckersten, G. Ekstrand, A.-K. Honerud, G. Jesson, G. Thorsén, T. Söderman and P. Andersson, *Clin. Chem.*, 2005, **51**, 1985–1987.
43 K. F. Buechler, *US pat.*, US 5458852 A, 1995.
44 D. J. Kinahan, S. M. Kearney, N. Dimov, M. T. Glynn and J. Ducree, *Lab Chip*, 2014, **14**, 2249–2258.
45 J. Siegrist, R. Gorkin, L. Clime, E. Roy, R. Peytavi, H. Kido, M. Bergeron, T. Veres and M. Madou, *Microfluid. Nanofluid.*, 2010, **9**, 55–63.
46 T. Thio, S. Soroori, F. Ibrahim, W. Al-Faqheri, N. Soin, L. Kulinsky and M. Madou, *Med. Biol. Eng. Comput.*, 2013, **51**, 525–535.
47 S. Soroori, L. Kulinsky, H. Kido and M. Madou, *Microfluid. Nanofluid.*, 2013, 1–13, DOI: 10.1007/s10404-013-1277-7.
48 A. Kazemzadeh, P. Ganesan, F. Ibrahim, M. M. Aeinehvand, L. Kulinsky and M. J. Madou, *Sens. Actuators, B*, 2014, **204**, 149–158.
49 M. C. R. Kong and E. D. Salin, *Anal. Chem.*, 2011, **83**, 1148–1151.
50 T. Brenner, T. Glatzel, R. Zengerle and J. Ducrée, A Flow Switch Based on Coriolis Force, *7th international conference on micro total analysis systems*, 2003, 5–9.
51 J. Kim, H. Kido, R. H. Rangel and M. J. Madou, *Sens. Actuators, B*, 2008, **128**, 613–621.
52 A. Kazemzadeh, P. Ganesan, F. Ibrahim, M. M. Aeinehvand, L. Kulinsky and M. J. Madou, *Sens. Actuators, B*, 2014, **204**, 149–158.
53 D. J. Acheson, *Elementary fluid dynamics*, Oxford University Press, 1990.
54 A. W. Adamson, *Physical chemistry of surfaces*, Wiley, 1990.
55 J. Chen, P. C. Huang and M. G. Lin, *Microfluid. Nanofluid.*, 2008, **4**, 427–437.
56 H. Cho, H.-Y. Kim, J. Y. Kang and T. S. Kim, *J. Colloid Interface Sci.*, 2007, **306**, 379–385.
57 A. Kazemzadeh, P. Ganesan, F. Ibrahim, S. He and M. Madou, *PLoS One*, 2013, **8**(9), e73002.
58 H. He, Y. Yuan, W. Wang, N. R. Chiou, A. J. Epstein and L. J. Lee, *Biomicrofluidics*, 2009, **3**, 22401.
59 S. E. Lin, *Microfluid. Nanofluid.*, 2010, **9**, 523–532.
60 J. Takagi, M. Yamada, M. Yasuda and M. Seki, *Lab Chip*, 2005, **5**, 778–784.
61 R. B. Bird, W. E. Stewart and E. N. Lightfoot, *Transport phenomena*, John Wiley & Sons, 2007.